ELSEVIER

Contents lists available at ScienceDirect

## Computational Materials Science

journal homepage: www.elsevier.com/locate/commatsci





# Vacancy-cluster and off-lattice metal-atom diffusion mechanisms in transition metal carbides

Rofiques Salehin a,\*, Xiaochuan Tang a, Gregory B. Thompson b, Christopher R. Weinberger a,c

- <sup>a</sup> Department of Mechanical Engineering, Colorado State University, Fort Collins, CO 80523, USA
- b The University of Alabama, Department of Metallurgical and Materials Engineering, 401, 7th Avenue, 285 Hardaway Hall, Tuscaloosa, Alabama 35487, USA
- <sup>c</sup> School of Advanced Materials Discovery, Colorado State University, Fort Collins, CO 80523, USA

## ARTICLE INFO

#### Keywords: Density functional theory Transition metal carbides Vacancies Diffusion

## ABSTRACT

Using *ab initio* simulations, we report potential metal atom diffusion mechanisms in the group IVB and VB transition metal carbides. By computing the metal vacancy formation energies of vacancy clusters, we find that a metal vacancy surrounded by six carbon vacancies is the lowest metal vacancy formation energy structure for the group IVB carbides while the lowest energy for the group VB carbides is a metal vacancy surrounded by two carbon vacancies. The vacancy cluster mechanisms reveal activation energies that are consistent with experiments in both TiC (group IVB) and TaC (group VB). We also report that an off-lattice diffusion mechanism, that is only energetically favorable in the group IVB transition metal carbides, has a lower formation energy than the regular vacancy cluster mechanism. This new mechanism shows lower formation energies for a given carbon vacancy concentration which indicates this off-lattice mechanism might be the most dominant metal-atom diffusion mechanism among the existing mechanisms proposed for the group IVB metal carbides.

## 1. Introduction

The transition metal carbides (TMCs) of the group IVB and VB elements have a complex mixture of covalent, metallic and ionic bonding. As a result, they possess some unique properties such as high melting temperatures, hardness and wear resistance enabling them to find applications as structural materials and coatings within nuclear reactors, aerospace applications, and propulsion systems [1,2]. Furthermore, their refractory nature places TMCs as a subset within the family of the Ultra High Temperature Ceramics (UHTCs). At equal parts metal (Me) and carbon (C), the TMCs adopt the rocksalt crystal structure where the metal atoms arrange themselves in an fcc lattice and the carbon atoms occupy the octahedral interstices. Two of these carbides, TaC and HfC, possess the highest melting temperatures of any binary compounds, 3930 °C and 3980 °C respectively [3]. Generally speaking, group IVB and VB TMCs have high micro-hardness (2500-2900 kg/mm<sup>2</sup>) and are able to withstand mechanical loading even at elevated temperature approaching 3000 °C [1]. Though considerable research has been undertaken in understanding several of these structure-property connections, there are still fundamental gaps in our understanding of the physical mechanisms that control their deformation behavior at elevated temperatures.

https://doi.org/10.1016/j.commatsci.2021.110713
Received 26 May 2021; Accepted 6 July 2021
Available online 27 July 2021
0927-0256/© 2021 Elsevier B.V. All rights reserved.

At elevated temperatures, most materials deform via a time dependent process known as creep which is empirically described under uniaxial loading by the equation:

$$\dot{\varepsilon} = A\sigma^n \exp\left(-\frac{Q_c}{k_B T}\right),\tag{1}$$

where  $\dot{e}$  the strain rate response, A is a prefactor,  $\sigma$  is the applied stress, n the stress exponent,  $Q_c$  the activation energy for creep,  $k_B$  Boltzmann's constant and T is temperature. Using this equation, several experimental creep studies have been performed on TMCs. For example, Miloserdin et al. determined the activation energy of creep for ZrC in the temperature range 2450–2810 K using standard constant load creep tests as  $5.51 \pm 0.95$  eV [4]. Steinitz reported the activation energy of tensile creep for TaC as  $7.37 \pm 1.3$  eV between 1960 °C and 2100 °C [5]. Keihn and Kebler [5,6] reported activation energies of creep in  $TiC_{0.96}$  to be between 5.6 eV and 7.64 eV depending on temperature (between 1638 and 1809 °C) and the load with evidence of two different creep regimes. Chermant et al. reported the compression testing on TiC and noted that the activation energy for creep at temperatures >2000 K is 7 eV [7]. Spivak et al. also reported the activation energy for creep in  $TiC_{0.47-0.97}$  was 3.30-7.59 eV [8]. Brizes examined tensile creep of NbC and noted

<sup>\*</sup> Corresponding author.

E-mail address: salehin@colostate.edu (R. Salehin).

that the activation energy was 5.77 eV at a temperature of 2100  $^{\circ}C$  [9]. More recently, Smith et al. performed bending tests of TaC, between 2500–2700  $^{\circ}C$  and HfC, between 2100–2300  $^{\circ}C$  and found the activation energy was 9.81  $\pm$  1.63 eV and 7.1  $\pm$  0.56 eV respectively [10]. Collectively, these activation energies are relatively high, ranging between 5 eV to 10 eV, indicating a substantive resistance to creep.

Given that creep could be limited by either carbon atom diffusion or metal atom diffusion, or both, it is important to quantify and understand the activation energies for diffusion in these materials. As noted above, at sufficiently high temperature ( $\sim 0.5~T_m$ ), the behavior of creep is likely dominated by diffusion [11]. For the TMCs, the slower of the two processes, metal atom or carbon atom diffusion, will then be the rate limiting process and dictate the activation energy for diffusion. The activation energies for carbon diffusion, using tracer diffusion methods, have been experimentally determined in five of the six TMCs including the carbon ranges of TiC<sub>0.97-0.47</sub>, ZrC<sub>0.97-0.92</sub>, VC<sub>0.92-0.75</sub>, NbC<sub>0.97-0.7</sub> and TaC<sub>1.0-0.99</sub> [12–18]. Here, the values range from 2.15–4.94 eV, which are generally smaller than the reported activation energies for creep noted above.

The activation energy for diffusion,  $Q_D$ , in a crystalline solid via the vacancy mechanism is traditionally the algebraic sum of the vacancy formation energy and migration energy. However, in the interstitial carbides the diffusion of carbon is more akin to interstitial diffusion so that the diffusion rate is related to the concentration and activation energy is solely to the migration energy barrier. Yu et al. determined the carbon vacancy formation, which are near zero, and migration energies in these carbides [19]. Their reported computational migration energy barriers for self-diffusion of carbon were 3.7 eV (TiC), 4.3 eV (ZrC), 4.8 eV (HfC), 3.0 eV (VC), 3.6 eV (NbC) and 4.0 eV (TaC) which agree reasonably well with the aforementioned activation energies for carbon diffusion [19]. This agreement suggests that the mechanism for carbon diffusion in the TMCs is a vacancy diffusion mechanism. However, the activation energies are low and are more likely representative of low temperature creep, i.e. creep below 0.5  $T_m$ .

It is evident from the values presented above that isolated carbon diffusion is often not the rate limiting step for creep at high temperatures  $(>0.5 T_m)$  since experimental activation energies (5–10 eV) frequently exceed the carbon diffusion values (3-6 eV). Thus, it stands to reason that metal atom diffusion is active at higher homologous temperatures. Nevertheless, to the author's knowledge, there are only three experimental studies on metal self-diffusion reported. Yu and Davis found the self-diffusion activation energy for  $^{95}\text{Nb}$  to be 6.22  $\pm$  0.17, 5.89  $\pm$  0.14,  $6.16 \pm 0.27$  eV in the temperature range 2097–2387 °C and carbon concentrations of 0.868, 0.834, 0.766 respectively [20,21]. Using the same tracer technique, Sarian determined the self-diffusion activation energy for <sup>44</sup>Ti diffusion in TiC<sub>0.97-0.67</sub> in the temperature range 1920–2215 °C as 7.64  $\pm$  0.16 eV [22] and found the values to be independent of concentration. Andeievskii et al. studied the Zr and Nb selfdiffusion in ZrC<sub>0.97-0.84</sub> and NbC<sub>0.97-0.78</sub> experimentally at 2400 °C and reported the activation energies to be 7.46 eV and 5.51 eV respectively [23]. These values are reasonably close to the activation energies observed in the high temperature creep experiments previously discussed. However, computational studies have demonstrated that the sum of the migration energy and formation energy of Ti vacancies in TiC are approximately twice the experimentally reported activation energies [24]. In the case of metal vacancies in the TMCs, the formation energy is large and positive and thus the activation energy for diffusion is the sum of a vacancy formation energy term and the migration energy barrier. This discrepancy in activation energies implies that the mechanism of metal atom self-diffusion in TiC is not via a simple (single) vacancy mechanism.

To provide additional insight into the vacancy migration mechanism and the discrepancy of activation energies, Razumovskiy et al. [25] considered the possibility that a metal atom vacancy moves in coordination with one more carbon vacancies and computed both the formation energies of metal–carbon atom vacancy clusters as well as the

migration energies of select clusters. These authors found that a metal vacancy surrounded by six carbon vacancies had the lowest formation energy, which has a more significant impact on the activation energy for diffusion than the migration energy. They also proposed a jump sequence of the vacancies to attain the lowest migration energy barrier. While these authors only investigated the group IVB carbides, they suggested that the same mechanisms must occur in the group VB carbides. Sun et al. also recently proposed an off-lattice diffusion mechanism by computationally studying Ti diffusion in TiC, considering the formation of metal atom at the interstitial position that is and is not surrounded by carbon vacancies [26]. While this mechanism provides very small migration energy barrier for the atom diffusion, the formation energy of such interstitial defect is very high ( $\sim$  9 eV) [26] for an isolated defect and ( $\sim$  4 eV) [27] for an vacancy-interstitial deflect complex.

To understand the metal self-diffusion mechanisms in the both groups of carbides, we performed *ab initio* atomistic simulations of the vacancy formation and migration energies in the group IVB and VB TMCs near the MeC<sub>1.0</sub> composition. We did not consider the elements Rf and Db from these two groups because they do not naturally occur and have short half-lives. We examined the formation energies of both isolated and clustered metal and carbon atom vacancies in the remaining group IVB and VB TMCs. Due to high computational cost, we choose one element from each of these groups (Ti from group IVB and Ta from group VB) to determine their migration energies for the various cluster mechanisms.

#### 2. Methodology

In this work, we utilized electronic structure density functional theory (DFT) as implemented in the Vienna Ab-initio Simulation Package (VASP) to perform all our simulations [28-30]. This included the use of the projector augmented-wave (PAW) pseudopotentials [31,32] to account for core-valence interactions and the Generalized Gradient Approximation (GGA) [33] to evaluate the exchange correlation energy as parameterized by Purdew-Burke-Ernzerhoff (PBE) [34]. The valence electrons directly simulation in this work include the Ti 3d<sup>2</sup>4s<sup>2</sup>, Zr 4d<sup>2</sup>5s<sup>2</sup>, Hf 5d<sup>2</sup>6s<sup>2</sup>, V 3d<sup>3</sup>4s<sup>2</sup>, Nb 4p<sup>6</sup>4d<sup>4</sup>5s<sup>1</sup>, and Ta 5d<sup>3</sup>6s<sup>2</sup>. Brillouin zone integration was performed using the Monkhorst-Pack integration scheme with a constant k-point density [35]. The choice of the number of valence electrons has a very small effect on the results reported here while the choice of the exchange correlation energies have a slightly larger impact. We choose to use the PBE exchange correlation function results here specifically because it has been used in previous studies to examine the diffusion in the transition metal carbides and is know to reproduce the lattice constants and cohesive energies of these materials [36,24–27,37,19,38]. The energy was sufficiently converged using a 12 imes 12 imes 12 integration scheme for the conventional eight atom unit cell of the B1 structure with a plane-wave cutoff energy of 450 eV. The total energy convergence criterion for the electronic and structural relaxations was set to  $10^{-5}$  eV and  $10^{-4}$  eV respectively which results in numerical errors that are smaller than the data points used in the figures. The Nudged Elastic Band (NEB) method was applied to estimate the migration energy barrier through the saddle point using a total of nine images [39].

We can classify the vacancy defects studied in this work broadly into two categories: vacancy clusters as proposed by Razumovskiy et al. [25] and vacancy-interstitial clusters. These two defect categories can be regarded as extensions to classical bound Schottky defects and bound Frenkel defects [40]. This concept is illustrated below in Fig. 1, which shows (a) a bound Schottky defect or bound vacancy pair, (b) a bound Frenkel defect or bound vacancy-interstitial pair, (c) a vacancy cluster and (d) a vacancy-interstitial cluster. Based on previous work [25], it is convenient to define the clusters by the number of total vacancies in the cluster and thus cluster in Fig. 1(a) is a di-vacancy pair while that shown in Fig. 1(c) is a tetra-vacancy cluster. Similarly, we classify the Fig. 1(b)

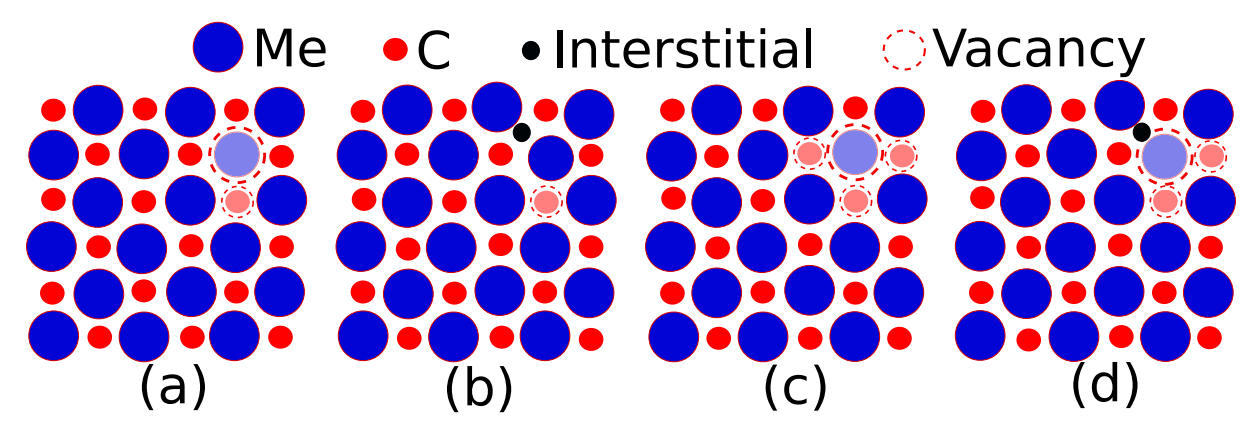


Fig. 1. Example schematic illustrating (a) bound vacancy pairs, (b) bound vacancy interstitial pairs, (c) bound vacancy clusters and (d) bound vacancy interstitial clusters.

as a vacancy-interstitial pair and Fig. 1(d) as a tri-vacancy interstitial cluster.

The defect formation energy was also approximated using the DFT supercell approach in which a sufficiently large number of atoms in the appropriate crystal structure, which is the B1 structure here, are simulated. In this method, the total energy of a supercell containing N atoms and one containing nominally the same number minus those required to form the defect are computed. Since we are dealing with binary compounds, we can readily write the energy in a short hand notation that reflects the number of atoms and total number of vacancies in the supercell as E(N-y-z,y,z). Here, N is the reference number of atoms in the defect free supercell, y is the number of metal vacancies ( $Me_v$ ), and z is the number of carbon vacancies ( $C_v$ ) in the TMC. The formation energy of a supercell can then be computed as:

$$E_f(yMe_v - zC_v) = E(N - y - z, y, z) + y \cdot \mu_{Me} + z \cdot \mu_C - E(N, 0, 0)$$
 (2)

where  $\mu_{Me}$  and  $\mu_{C}$ , of Eq. (2), are the chemical potentials of the transition metals and carbon, respectively. In DFT, it can be difficult to compute the chemical potential of the atoms precisely and sometimes the peratom energy of the pure states is used, which would be the energy of the pure metal and graphite here. In this work, we compute the chemical potentials by fitting the cohesive energies to the convexhull between the nearest subcarbide on the convex hull and the B1 structure. In the case of vanadium and niobium carbides, the B1 structure does not lie on the convex hull so we use the nearest subcarbide (Nb $_6$ C $_5$  and V $_6$ C $_5$ ) and graphite. These chemical potentials are therefore approximate as they should be continuous at finite temperature but this approach does provide a direct measure of how far the defected structures lie above the convex hull and thus accurately represent the defect formation energies. The cohesive energies and chemical potentials for these transition metal carbides can be found in Table 1. More details on how the chemical potential can vary in these systems and uncertainties associated with these approximations can be found in the Supplemental Information.

In order to compute these defect formation energies, it is necessary to establish a supercell that is sufficiently large to eliminate periodic ef-

fects. To this end, we computed defect formation energies, to be discussed below, in various sized supercells. These size convergence studies included supercells of the two-atom primitive unit cell with  $2\times N^3$  atoms and eight-atom conventional unit cell with  $(2\,N)^3$  atoms where N is the number of repetitions of the unit cell in each direction  $(N\times N\times N)$  supercell). We also used the Special Quasi-random Structure (SQS) to create optimal periodic supercells with an arbitrary number of atoms in between the primitive and conventional supercells [41]. Convergence of the per-atom energy for different supercells with point defects (i.e. vacancies) within the cell were tested at the chosen constant k point density. The supercell convergence can be found in the Supplemental Information, but these results show that a supercell with 128 atoms prior to defect formation is more than sufficient for our simulations, which is used in the rest of this paper.

## 3. Results and discussion

#### 3.1. On-lattice vacancy diffusion

## 3.1.1. Defect formation and binding energies

Since modeling has previously demonstrated that the formation energies of isolated metal vacancies in TiC and ZrC exceed the activation energy for diffusion [24], understanding the formation energies of extended defects, especially vacancy clusters, is critically important. To this end, we must understand the formation energies and binding energies of different vacancy configurations. The first thing we investigated is the formation energy of isolated vacancies, both metal  $E_f^{iso}(Me_v)$  and carbon  $E_f^{iso}(C_v)$ , in the group IVB and VB carbides as well as the energy to bind them together. The formation energy of isolated metal and carbon vacancies as well as the binding energy of a metal and carbon vacancy in the 1st nearest neighbor (NN) shell for all the six group IVB and VB carbides are shown in Table 2. The formation energy of an isolated metal vacancy, calculated using Eq. (3a), is 7.67 eV and 2.65 eV in TiC and TaC respectively. The simulations of the isolated carbon vacancies lie on the convexhull within the accuracy of our simulations and

**Table 1** Cohesive Energies ( $E_{Coh}$ ) and Chemical Potentials ( $\mu$ ) of Metal and Carbon in their respective metal carbides (MeC).

Compounds	Cohesive Energy of Metal Carbide $E_{Coh}^{MeC}$ (eV)	Cohesive Energy of Carbon $E_{Coh}^{C}(eV)$	Cohesive Energy of Metal rich Carbide $E_{Coh}^{Me_xC_y}$ (eV)	Chemical Potential of Metal $\mu_{Me}^{MeC}(eV)$	Chemical Potential of Carbon $\mu_C^{MeC}(eV)$
TiC	14.71	7.85	94.66	$-6.40\pm0.00$	$-8.31 \pm 0.00$
ZrC	15.82	7.85	102.12	$-7.19\pm0.02$	$-8.63\pm0.02$
HfC	16.26	7.85	104.80	$-7.27\pm0.01$	$-8.99\pm0.01$
VC	14.01	7.85	77.22	$-6.33\pm0.00$	$-7.85\pm0.00$
NbC	15.72	7.85	86.98	$-7.96\pm0.00$	$-7.85\pm0.00$
TaC	17.23	7.85	95.39	$-9.26\pm0.01$	$-7.96\pm0.01$

**Table 2**Formation and Binding energies of group IVB and VB transition metals carbides.

Compounds	$E_f^{iso}(Me_v)$ (eV)	$E_f^{iso}(C_v)$ (eV)	$E_f^{Me_v-C_v cluster}(Me_v)$ (eV)	$E_f^{Me_{\nu}-6C_{\nu}cluster}(Me_{\nu})$ (eV)	$E_b(Me_{\nu}-C_{\nu})$ 1st NN (eV)
TiC	7.67	0.00	6.22	2.99	-1.45
ZrC	8.29	0.00	6.76	2.70	-1.53
HfC	8.64	0.00	7.10	2.95	-1.54
VC	3.59	-0.89	3.22	4.30	-0.37
NbC	3.29	-0.38	3.04	3.62	-0.25
TaC	2.65	0.00	2.49	2.78	-0.16

thus the formation energies are zero for both TiC and TaC. If the carbon and metal vacancies are bound together, for example in the 1st NN shell, then the overall formation energy changes by the binding energy,  $E_h(Me_v - C_v)$ . If the binding energy is negative, as defined in Eq. (4), there will be an attractive interaction between the vacancies lowering the overall formation energy and vice versa. The binding energy of bound Ti-C vacancies in TiC and Ta-C vacancies in TaC are  $-1.45\,\text{eV}$  and −0.16 eV respectively (Table 2) as computed from our DFT simulations. If we assume carbon vacancies already exist in the structure, which is common in these TMCs since their phase field covers a wide stoichiometry, the binding energy should effectively lower the formation energy of the metal vacancy. Thus, the formation energy of Ti and Ta vacancies in the 1st NN of a carbon vacancy are 6.22 eV and 2.49 eV, respectively (Eq. (5)). These values are representative of differences between the two groups; the other group IVB metal carbides also have at least a three times larger  $Me_{\nu}-C_{\nu}$  binding energy than the group IVB metal carbides, as listed in Table 2.

$$E_f^{iso}(Me_v) = E(N-1,1,0) + \mu_{Me} - E(N,0,0)$$
(3a)

$$E_f^{iso}(C_v) = E(N-1,0,1) + \mu_C - E(N,0,0)$$
 (3b)

$$E_b(Me_v - C_v) = E(N-2, 1, 1) + E(N, 0, 0) - E(N-1, 1, 0) - E(N-1, 0, 1)$$
(4)

$$E_f^{Me_v - zC_v cluster}(Me_v) = E_f(Me_v - zC_v) - z \cdot E_f(C_v)$$
(5)

Since the presence of one carbon vacancy in the metal vacancies 1st NN shell reduces the energy required to form the metal vacancy, we expect that the formation energy of metal vacancies can be reduced further in the presence of additional carbon vacancies as originally pointed out by Razumovskiy et al. [25]. The agglomeration of such vacancies would form a vacancy cluster. Since a metal atom has six 1st NN carbon atoms, it is possible to form up to six carbon vacancies around the metal vacancy. In this case, the binding (or interaction) energy between the carbon vacancies also contributes to the total binding energy of a vacancy cluster and thus formation energy of metal vacancies in the cluster. Thus, it is important to understand how carbon vacancies interact. We computed the binding energy of two C-C vacancies as a function of their relative positions the first to sixth nearest neighbor shells as shown in Fig. 2 and in the Supplemental Information while Fig. 2 shows the  $C_{\nu} - C_{\nu}$  binding energies for the two carbides studied the most extensively in this work (i.e. TiC and TaC). The  $C_{\nu}$  –  $C_{\nu}$ binding energy for TiC and TaC is generally positive and thus repulsive for almost every nearest neighbor distance except the third nearest neighbor shell. However, the high attractive binding energy ( $\sim -1.5\,\text{eV}$ ) of  $Me_{\nu}-C_{\nu}$  in the group IVB would overpower the  $C_{\nu}-C_{\nu}$  repulsive binding energy ( $\sim 0.2$  eV) and therefore result in a strong potential for carbon vacancy cluster formation around the metal vacancy [25]. Our reported energies and conclusions for the group IVB TMCs match those reported by Razumovskiy et al. [25]. However, a similar clustering of carbon vacancies around a group VB metal vacancy is not nearly as favorable since the  $Me_{\nu}-C_{\nu}$  binding energy is not much larger in magnitude than the repulsive  $C_{\nu}$  – $C_{\nu}$  binding energy. This suggests the formation of clusters of multiple vacancies should favorable in the group IVB carbides but cast doubt of its favorability in the group VB carbides.

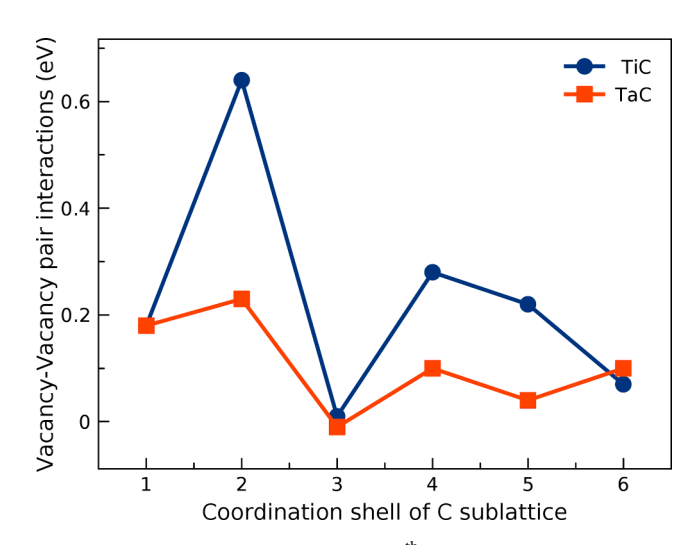


Fig. 2.  $C_v$ - $C_v$  binding energy from the 1st to  $6^{th}$  nearest neighbor in carbon sublattice in TiC and TaC with no metal vacancies.

To better understand the clustering mechanism and find the lowest required energy to form a metal vacancy, we consider all the possible carbon vacancies around a metal vacancy in its 1st NN shell, including the number and arrangement of those vacancies. Fig. 3(a) shows the atomic configuration of all the six potential carbon vacancies in the 1st NN of a metal vacancy. When there are one, five and six carbon vacancies, there is one indistinguishable microstate (or configuration) associated with those vacancy clusters. When there are two to four carbon vacancies, there are two different microstates and thus two energies for each number of vacancies. For two carbon vacancies, the carbon vacancy configurations either form a triangle (e.g. positions 1 and 2 of Fig. 3(a)) or a line (positions 1 and 3). For three carbon vacancies, they could be in the same plane (positions 1, 2, and 3) or form out of plane (positions 1, 2, and 5). Similarly, for four vacancies, all fourcarbon vacancies could be oriented in the same plane (positions 1–4) or out of plane (positions 1, 2, 5, and 6). Fig. 3(b) and 3(c) shows the formation energies of the metal vacancy as a function of the number of bound carbon vacancies, including all the arrangements of each vacancy cluster, for the group IVB and VB TMCs. As the number of carbon vacancies increases from zero to six, the vacancy formation energy of Ti in TiC reduces continuously from 7.67 eV to 2.99 eV. If one additional carbon vacancy is added to the metal's 2nd NN shell after the 1st NN shell is filled with six carbon vacancies, the formation energy increases. We also found that, as shown in Fig. 3(c), the metal vacancy formation energy of Ta in TaC decreases from 2.65 eV to 2.36 eV as the number of carbon vacancies increases from zero to two (Supplemental Information). For one additional carbon vacancy in the 1st NN shell, the overall  $C_{\nu}-C_{\nu}$  repulsive interaction overcomes the  $Me_{\nu}-C_{\nu}$  binding energy, which results in an overall increase in the metal formation energy. This increase of metal formation energy continues for additional carbon vacancies in the 1st NN of the metal and when all six 1st NN of Ta is full of carbon vacancies, the metal formation energy increases to its highest value, i.e. 2.78 eV. Hence, the lowest formation energy for a metal

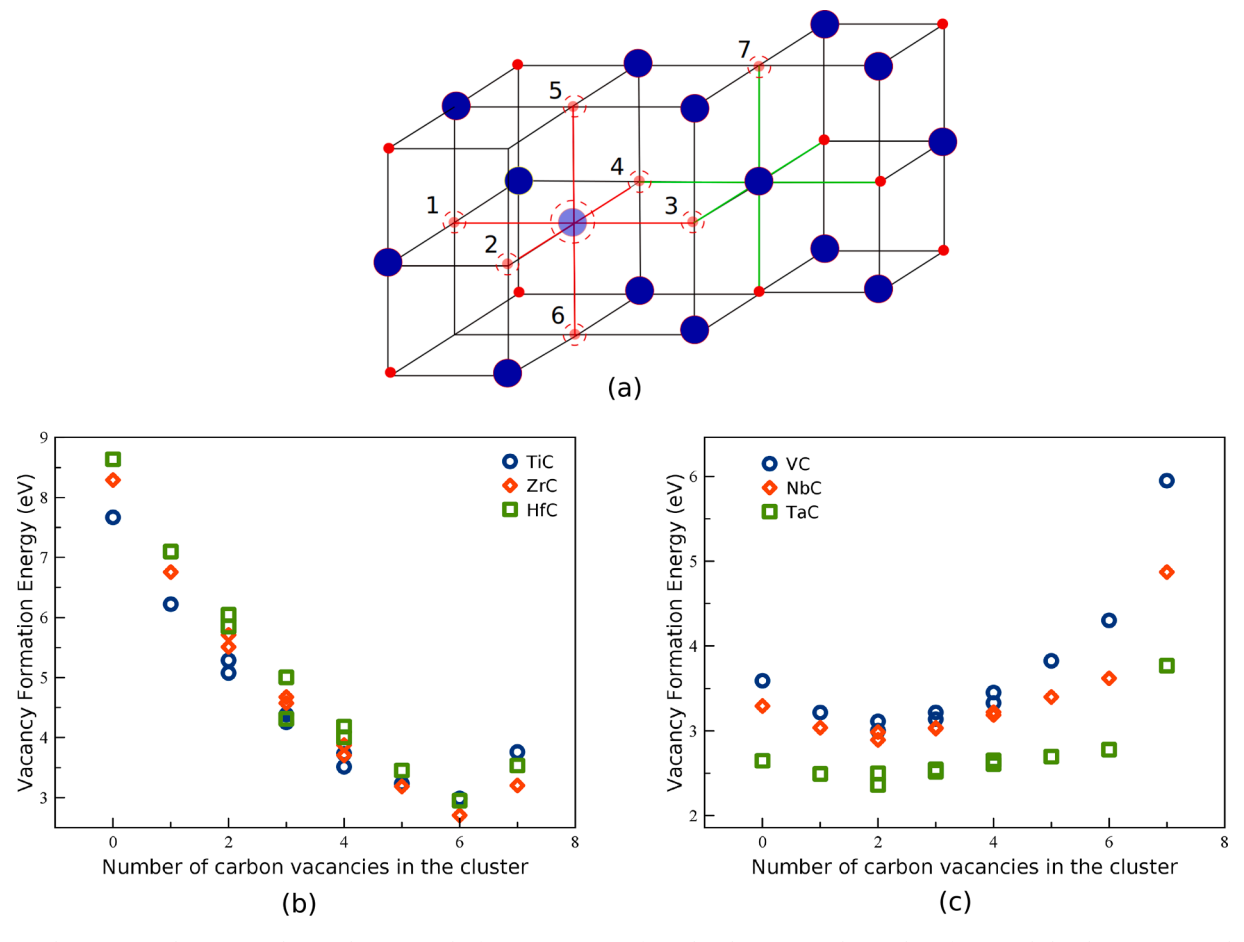


Fig. 3. (a) Carbon vacancy cluster around a metal vacancy. The formation energy of metal with respect to the number of surrounded carbon vacancy in (b) TiC and (c) TaC.

vacancy in TiC and TaC is the metal formation energy with six carbon vacancies and two carbon vacancies in the metal's nearest neighbor, respectively. Similar trends are observed in all the group IVB and VB TMCs as shown in Fig. 3 and Table 2. Note that these conclusions for TiC, ZrC, HfC, and TaC have been reported before in part by Razumovskiy et al. [25,38], and Tang et al. [36] but here we demonstrate their generality across the group IVB and VB TMCs.

## 3.1.2. Migration mechanism

In the previous section, we examined the vacancy formation energy of a metal vacancy in a vacancy cluster, which contributes only part of the activation energy. The other contribution to the overall activation energy is the migration energy barrier. In the following sections we examine the different migration mechanism for selected vacancy clusters. With these migration barriers and the previously computed formation energies, we compute the effective activation energies of specific migration mechanism to help understand the metal atom diffusion mechanisms in group IVB and VB TMCs with a summary of these findings shown in Table 3.

Single vacancy.

The first set of migration mechanisms we investigated is the single vacancy migration mechanism, for both the metal and carbon vacancies. There are two possible paths one can consider for this set of mechanisms. The first corresponds the atom swapping positions with the nearest vacancy along a  $<\!110>$  direction in the B1 structure. The second corresponds to atomic motion through the adjacent tetrahedral interstice. Fig. 4(a) shows these two paths for carbon atom migration where the path shortest distance (SD) corresponds to first path while TI corresponds to the second through the tetrahedral interstice (TI). For the

**Table 3**Activation Energies for the on-lattice migration paths considered in this paper.

		$E_f$		$E_m$		Q
	TiC	TaC	TiC	TaC	TiC	TaC
Experiment [5,22]					7.64	7.37
Single Vacancy	7.67	2.65	5.40	5.31	13.07	7.96
Di-vacancy Seq-YYY	6.22	2.49	3.95	3.98	10.17	6.47
Di-vacancy Seq-YNY	6.22	2.49	5.22	5.38	11.44	7.87
Di-vacancy Sim-<110>{100}	6.22	2.49	5.62	5.72	11.84	8.21
Di-vacancy Sim-<110>{110}	6.22	2.49	6.89	7.64	13.11	10.13
$Me_{\nu}-6C_{\nu}$ cluster	2.99	2.78	3.63	5.05	6.62	7.83

migration of an isolated metal atom, the tetrahedral interstice is very energetically unfavorable so we do not report on the energetics here. Figs. 4(c) and 4(d) shows the minimum energy paths as found by NEB simulations for the aforementioned metal migration SD path and carbon migration for both the SD and TI paths in TiC and TaC.

Since the activation energy of mass diffusion is effectively determined by the largest migration barrier for all necessary atomic jumps, it is important to identify this maximum. The energy barrier for Ti migration in TiC and Ta migration in TaC is 5.40 eV and 5.31 eV, respectively as shown in Fig. 4(c). Similarly, the energy barrier of carbon diffusion for the SD and TI paths in TiC are 3.79 eV and 3.55 eV respectively, while the barriers for Ta migration in TaC are 3.99 eV and 4.86 eV respectively. The energy barriers for carbon diffusion in TiC and TaC clearly indicate that the migration of isolated carbon atoms in TiC prefer the path through the nearest tetrahedral interstice whereas carbon migration in TaC prefers SD path primarily along the <110>

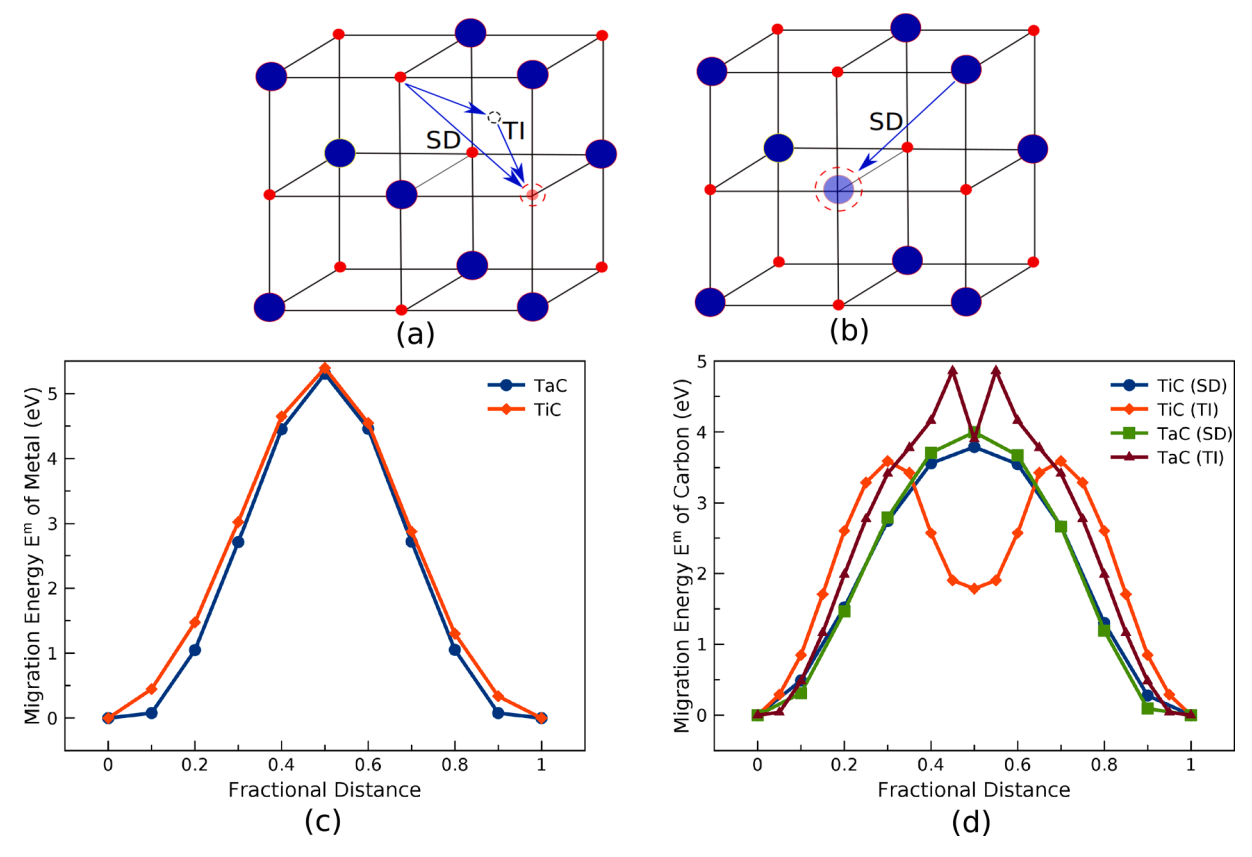
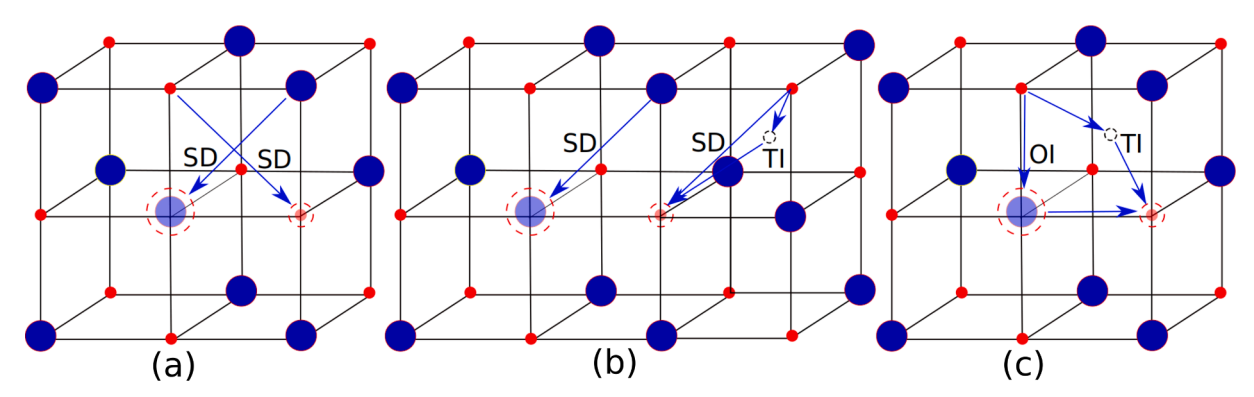


Fig. 4. Single vacancy jump mechanism (a) for carbon and (b) metal in TiC and TaC. The migration energy barrier for (c) metal through the shortest distance and (d) carbon through the shortest distance and nearest tetrahedral interstitial position.

direction. However, all of the carbon migration paths studied in TiC and TaC have lower energy barriers than the migration of their respective metal vacancies. Thus, the overall activation energy for mass diffusion that occurs by a combination of isolated carbons and metal atoms is found by adding the energy required to form an isolated metal vacancy to the energy required for metal atom vacancy migration. This results in an activation energy for mass diffusion in TiC and TaC of 13.07 eV and 7.96 eV respectively. This mechanism provides a similar activation energy for Creep in TaC (7.4–9.8 eV), but much higher activation energy for Ti diffusion in TiC (7.64 eV) [22]. Thus, the single vacancy migration mechanism described above can be considered as a potential mechanism for metal atom migration in TaC (assuming the activation energy of migration of Ta in TaC equivalent to the aforementioned activation energy for creep) but not for TiC.

## Di-vacancy.

The di-vacancy mechanism is a vacancy diffusion mechanism whereby a metal and carbon vacancy bound in their 1st NN move cooperatively [25]. The migration of a di-vacancy pair can occur either (a) sequentially or (b) simultaneously (i.e. molecular diffusion [25]). For sequential migration, there are many different possible paths in which the atoms can migrate so that the starting and ending configuration have the same bound di-vacancy configuration. The first sequential mechanism we consider preserves the 1st NN coordination of the two vacancies during the sequential jump process (*Seq-YYY*, the naming convention is explained in S2). This mechanism is shown in Fig. 5(a) where the migrating vacancies appear to cross paths, although the same mechanism can occur by the atoms moving in parallel as well as shown in 5b when the metal atom moves first. Another sequential mechanism occurs



**Fig. 5.** (a) The *Seq-YYY* mechanism along the shortest distance (SD) path when metal and carbon vacancies cross paths. (b) The *Seq-YYY* mechanism where the metal atom migrates first in the parallel path or *Seq-YNY* mechanism when carbon atom migrates first. (c) The tetrahedral interstitial (TI) and metal vacancy (OI) path for carbon migration.

when the migration of the bound vacancies occurs such that in the intermediate state puts the metal and carbon vacancy in their third nearest neighbor shell as shown in Fig. 5(b) when the carbon atoms moves first along the SD trajectory (*Seq-YNY*).

As was noted in the case of the single vacancy diffusion mechanism, it is possible for the carbon atom to move to other locations during its migration in the sequential process. Due to the presence of a metal vacancy there are now two possible new paths that do not follow the SD path along the <110> direction, one through the tetrahedral interstice (TI path) and one through the metal (octahedral location) vacancy (OI path). These alternative carbon migration paths are shown in Fig. 5(c).

Similarly, there are several different simultaneous migration paths possible. Here, we consider the two most likely, as shown in Fig. 7(a)–(b). The di-vacancy, which is bonded along a <100> direction, can migrate simultaneously along either a <110> direction in a {100} plane (aka Sim-<110>{100}) or a <110> direction in the {110} plane (aka Sim-<110>{110}). These paths are shown in Fig. 7(a) and 7(b) respectively.

As part of the sequential 1st NN diffusion mechanism, the migration barriers for carbon vacancy diffusion through the three previously described paths (i.e. SD, TI, and OI) are shown in Fig. 6(a) and 6(b) for TiC and TaC respectively. For TiC, in Fig. 6(a), the energy barrier for carbon vacancy diffusion via the SD, TI, and OI trajectories are 2.33 eV, 2.02 eV and 2.07 eV respectively. Similarly, for TaC, in Fig. 6(b), we found the lowest energy barrier for carbon via the SD, TI and OI trajectories are 3.82 eV, 3.18 eV and 3.98 eV respectively. These barriers clearly indicate the most favorable migration path of carbon vacancy migration in both TiC and TaC is carbon migration through the

tetrahedral interstice.

What is perhaps more interesting is that the results in Fig. 6(a) show two new metastable positions in TiC (path OI and TI, at a fractional distance of 0.5) have lower energy than any previously reported carbon vacancy configuration. The metastable position along the OI path has an energy that is 0.89 eV below its starting position, i.e. the formation energy of a standard carbon vacancy. Thus, a carbon atom at this metastable position would have a substantially lower vacancy formation energy than a normal carbon vacancy. Furthermore, along the TI trajectory, the calculations show another negative metastable position. The tetrahedral interstice is 0.30 eV below the starting configuration. These results indicate that the original on-lattice vacancy positions are not the most stable vacancy configurations. We will investigate this in detail in the next section. Nevertheless, it is worth noting that in our calculations we used the largest barrier between meta-stable positions for each of these paths in the calculations reported above.

The migration energy of Ti in TiC and Ta in TaC for the SD trajectory are shown in Figs. 6(a) and 6b) and are 3.95 eV and 3.98 eV respectively. Since the metal atom migration energy barrier is higher, the metal atom migration is the rate limiting step in the overall sequential diffusion mechanism. Thus, the activation energy for metal atom diffusion via the Seq-YYY mechanism is found by adding the migration energy for a carbon atom by preserving the 1st NN coordination to the energy of the metal atom migration resulting in an activation energy of 10.17 eV and 6.47 eV for TiC and TaC respectively, see Table 3. This result is a significant reduction in the activation energy for diffusion as noted by Razumovsky et al. in TiC [25], however our carbon diffusion path is different than that reported by Razumovsky.

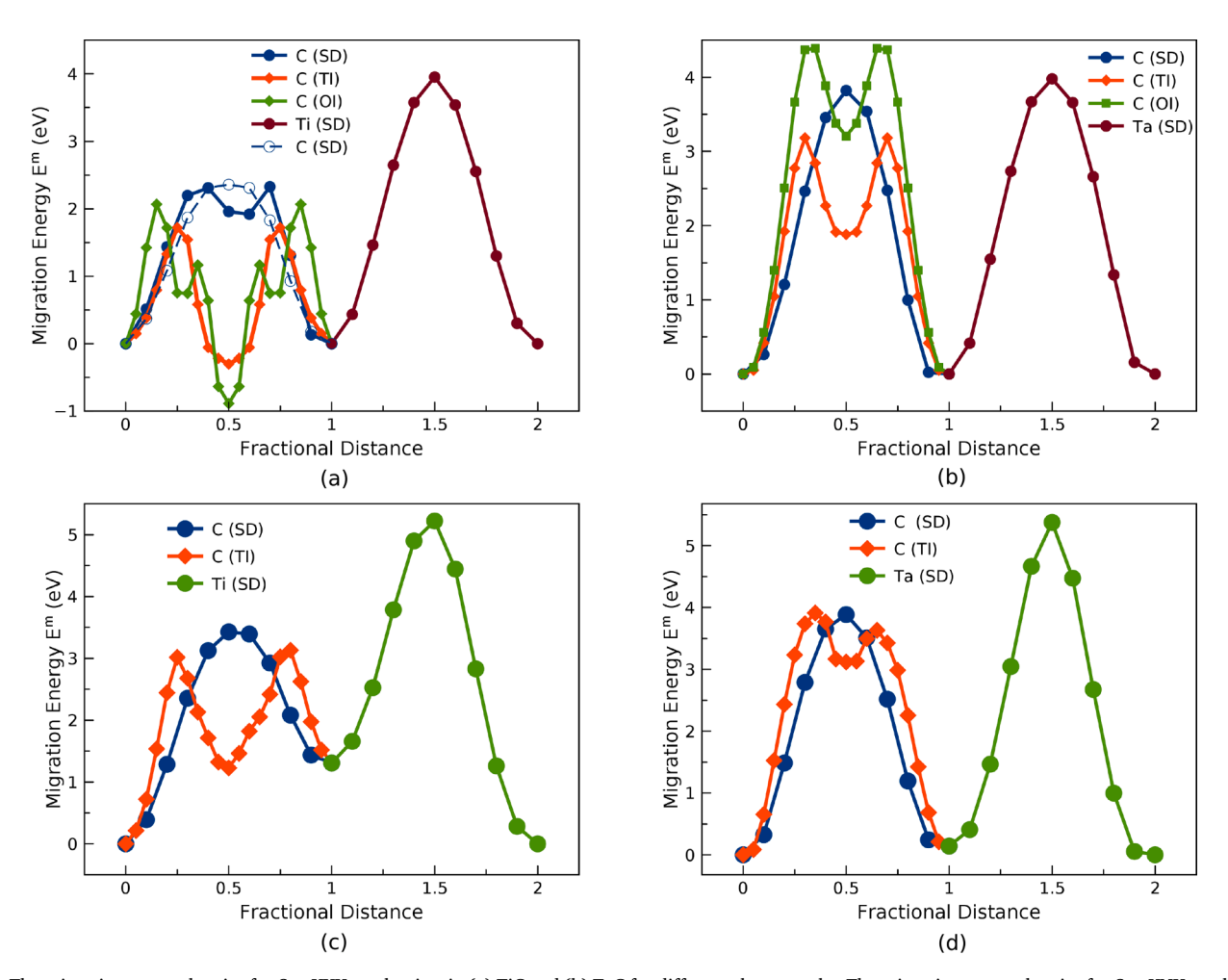


Fig. 6. The migration energy barrier for Seq-YYY mechanism in (a) TiC and (b) TaC for different chosen paths. The migration energy barrier for Seq-YNY mechanism in (c) TiC and (d) TaC.

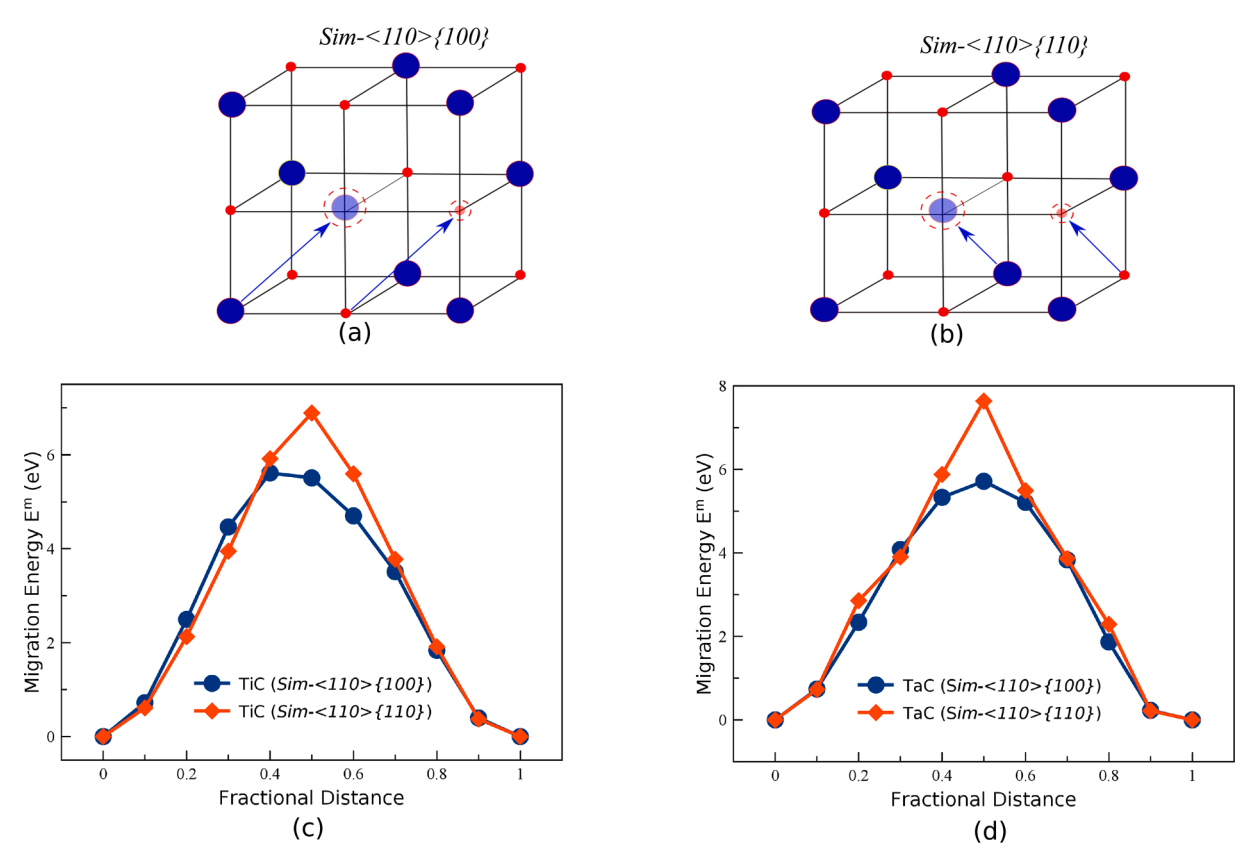


Fig. 7. Simultaneous jump mechanism for (a) Sim-<110>{100} and (b) Sim-<110>{110}. The migration energy barrier for (c) TiC and (d) TaC for these different simultaneous jump mechanisms.

For the sequential migration process in which the intermediate state puts the carbon vacancy in the metal atom's 3<sup>rd</sup> NN shell can proceed by carbon atom motion either through the SD trajectory and TI trajectory as shown in Fig. 5(b) and 5(c). The minimum energy paths for these atomic trajectories are shown in Fig. 6(c) and 6(d). The migration energy barrier for carbon (Fig. 6(c) and 6(d)) via the SD trajectory is 3.42 eV and 3.89 eV for TiC and TaC, respectively. The TI path results in a barrier of 3.13 eV and 3.91 eV for TiC and TaC, respectively. The tetrahedral interstice is again found to be a metastable position, similar to what was found before, but these metastable positions are higher energy than the original carbon position. Despite the higher energy metastable position, migration through the tetrahedral interstice is still lower than the SD trajectory.

Fig. 6(c) and 6(d) shows the minimum energy paths for the metal atoms resulting in energy barriers of 5.22 eV and 5.38 eV for TiC and TaC, respectively. Clearly, the metal atom migration energy barrier is the rate limiting energy barrier for *Seq-YNY* migration mechanism. Thus, the activation energy for *Seq-YNY* mechanism is 11.44 eV and 7.87 eV for TiC and TaC, respectively. Note that activation energies for the *Seq-YNY* mechanism is lower than the single vacancy mechanism but is less favorable than the *Seq-YYY* mechanism.

Fig. 7(c) and 7(d) shows the minimum energy paths for the *Sim*<110>{100} and *Sim*-<110>{110} mechanisms. The energy barriers associated with these paths are 5.62 eV and 5.72 eV for the *Sim*-<110>{100} paths and 6.89 eV and 7.64 eV for the *Sim*-<110>{110} for TiC and TaC, respectively. These values are obtained by terminating the simulations after the energy plateaus after the conclusion of a large number of relaxation steps, which is typically around 60 steps. However, if the simulations are continued for a larger number of ionic steps, well over 100, all these simulations break into different types of sequential atomic steps that we have already described previously. Thus, the sequential paths are not actually stable vacancy migration paths. If we

add the aforementioned migration barriers we obtained to the metal atom vacancy formation energy computed for the metal–carbon divacancy, we obtain activation energies for diffusion of 13.11 eV and 10.13 eV for Sim- $<110>\{100\}$  and 11.84 eV and 8.21 eV for the Sim- $<110>\{110\}$ , see Table 3. This demonstrates that the simultaneous migration paths are not only unstable in our simulations but also possess a higher energy than the sequential paths.

Cluster

The di-vacancy mechanism provides a lower activation energy than the single vacancy migration mechanism primarily because of the binding energy associated with the  $Me_{\nu}-C_{\nu}$  vacancies. The effect of the cluster on the migration energy barriers is generally weak. Therefore, Razumovskiy et al. [25] originally proposed that since the  $Me_{\nu}-6C_{\nu}$  vacancy cluster has the lowest formation energy (in TiC and ZrC), it should have the lowest activation energy for diffusion. In this section, we investigate the same mechanism to compare such effects between TiC and TaC.

Fig. 8(a) shows a vacancy cluster comprised of one metal vacancy surrounded by six carbon vacancies in the metal's 1st NN. The figure also indicates the jump sequence of atoms for cluster migration: 1–2–3–4–5–6–7. The straight lines shown in Fig. 8(a) indicate that the atomic jump does not find a metastable position while moving along the minimum energy path. Similarly, the jump depicted in Fig. 8(a) with a curved line indicates the moving atom finds a metastable position while following the chosen path. Fig. 8(a), and the results of the minimum energy path in Fig. 8(b), indicates that when a carbon atom moves with a metal vacancy in its 1st NN shell, the minimum energy path has a metastable position. This behavior is consistent with our observations of carbon atom migration for the di-vacancy pair noted above where the metal atom vacancy created new metastable positions.

Fig. 8(b) shows that the migration energy barrier of jumps 1, 2, 3, 4, 5, 6, and 7 in TiC is 3.63 eV, 3.04 eV, 3.58 eV, 2.29 eV, 2.48 eV, 2.72 eV

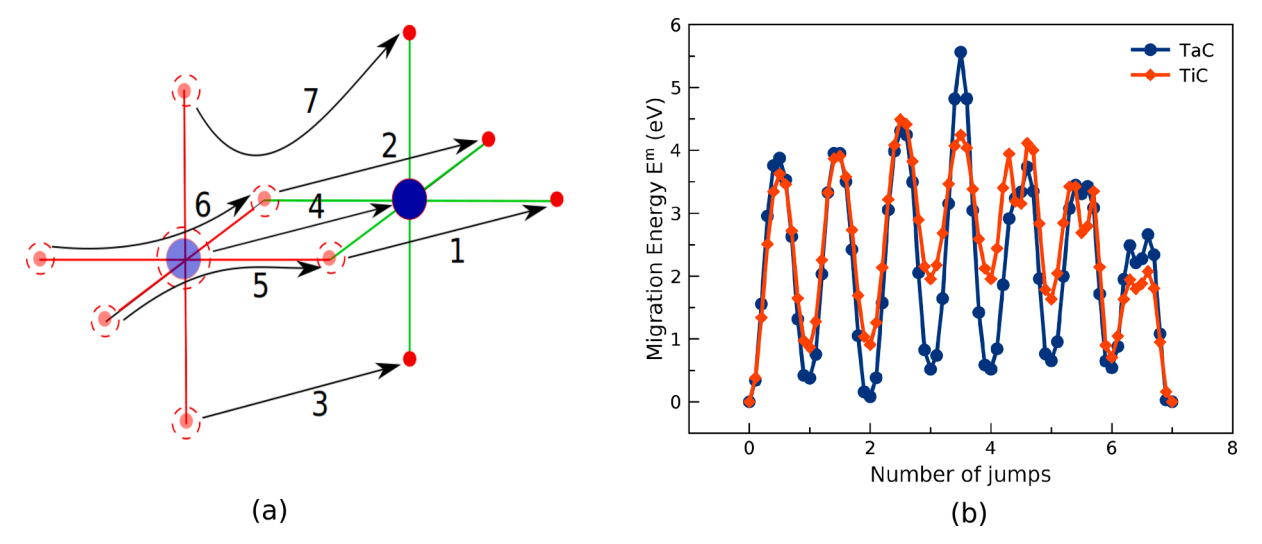


Fig. 8. (a) Cluster migration mechanism in TiC and TaC along the shortest distance path. (b) The migration energy barrier for TiC and TaC in  $Me_{\nu}-6C_{\nu}$  vacancy cluster.

and 2.07 eV respectively. Here, the rate limiting step is the migration of a carbon atom with an energy barrier of 3.63 eV. For TaC, the energy barrier for the atomic jumps are 3.88 eV, 3.87 eV, 4.22 eV, 5.05 eV, 3.22 eV, 2.91 eV and 2.66 eV for the sequential jumps, respectively. In this case, the Ta migration of 5.05 eV is the rate limiting step of migration. Thus, the activation energy for carbon dominated vacancy cluster migration in TiC is 6.62 eV whereas for metal dominated vacancy cluster in TaC is 7.83 eV.

To date, the simulated vacancy cluster mechanism in TiC has the computed lowest activation energy (6.62 eV, Table 3), which is below the activation energy observed experimentally (7.64 eV) [22]. The cluster mechanism studied here also uses the shortest distance paths for all paths and examining interstitial or octahedral positions might further lower the values in TiC. However, as pointed out by Tang et al. [36], this mechanism is very unlikely and does not contribute significantly in near stoichiometric carbides. The variation in activation energy for TaC for all the mechanisms discussed so far is not significant and are all close to the experimentally determined activation energy for creep (7.4–9.8 eV) [5]. As pointed out by Tang et al., the most relevant mechanism for mass diffusion in TaC is the di-vacancy mechanism which we have already studied. In comparison, the most relevant mechanism in TiC would be  $Ti_{\nu} - 4C_{\nu}$  and  $Ti_{\nu} - 5C_{\nu}$  vacancy clusters. This suggests that further studies of the  $Ti_{\nu}-4C_{\nu}$  and  $Ti_{\nu}-5C_{\nu}$  clusters would be warranted. However, our results have already demonstrated that new interstice positions are more energetically favorable than the clusters as suggested by Razumovskiy et al. [25] and thus we turn our attention to study these vacancy mechanisms.

## 3.2. Off-lattice vacancy diffusion

## 3.2.1. Defect formation energies

As demonstrated in our NEB simulations, one of the main findings of the previous section is that it is possible for a carbon atom near a metal vacancy to find positions that are energetically more favorable than the on-lattice position of that carbon atom. These off-lattice carbon positions are approximately the tetrahedral interstices in the B1 structure near the vacancies created by the metal atom. In order to establish the lowest formation energy, we systematically checked all the nearest tetrahedral and octahedral interstices of a metal atom vacancy. Furthermore, since previous analysis demonstrated that the number of carbon vacancies influences the formation energy, we also investigated these potential off-lattice sites for a total carbon vacancy concentration between zero and two carbon vacancies.

Fig. 9 shows the different possible tetrahedral interstices around a metal atom prior to lattice distortion for a single, double and triple carbon atom vacancy cluster. In this new defect, when a carbon atom is displaced from its on-lattice position to an interstitial position, it creates both a carbon interstitial and vacancy pair. For example, if we start with just a single metal vacancy, Fig. 9(a), and then displace a carbon atom from its lattice position to one of the interstitial positions, we create a metal atom vacancy plus carbon vacancy-interstitial pair. We denote this type of defect as a  $Me_v - C_v - I$  defect. Thus, if Fig. 9 represents only a single interstitial, we would denote the defects in Fig. 9(a)–(c) as  $Me_v - C_v - I$ ,  $Me_v - 2C_v - I$  and  $Me_v - 3C_v - I$  type defects.

The relative change of energy due to a carbon atom in the off-lattice position is calculated and listed on Table 4 for all the six group IVB and VB carbides. For  $Me_v - C_v - I$  and  $Me_v - 2C_v - I$  defect clusters, the change of energy is calculated relative to a single metal vacancy and di-vacancy, respectively. For the  $Me_v - 3C_v - I$  defect, the change of energy is relative to the triangle shaped configuration of the tri-vacancy, i.e. the most stable tri-vacancy configuration. A negative energy difference indicates microstates with a more favorable off-lattice positions. For these off-lattice positions, the formation energy required to form a metal vacancy will be reduced by the amount listed in Table 4 relative to the most stable on-lattice position.

Table 4 shows that, for a single metal vacancy, the tetrahedral interstice labeled as 3 in Fig. 9(a) reduces the energy the most for the group IVB carbides and thus is the most energetically favorable. Similarly, for a metal vacancy with one or two carbon vacancies in its nearest neighbor shell, the lowest energy state is when the carbon atom occupies the tetrahedral positions 3 and 2 as shown in Fig. 9(b) and 9(c), respectively. Note, the tetrahedral sites in TaC and NbC are not energetically more favorable. VC does have slightly lower energies and appears more similar to the group IVB carbides, but VC is not thermodynamically stable ( $V_8C_7$  forms instead) and VC is only shown here for completeness. Therefore, we can conclude that, the presence of a metal vacancy in the group IVB carbides will lead to energetically favorable off-lattice sites for the carbon atoms that are likely important for mass diffusion while the group VB carbides do not exhibit this behavior.

These results raise an important question regarding the origin for the decrease in energy associated with carbon atoms moving to tetrahedral interstices in the group IVB carbides as compared with the group VB carbides. Some of the trends can be understood by examining the formation energies shown in Table 4. First, we note that the removal of the metal atom breaks the covalent bonds between the metal and carbon

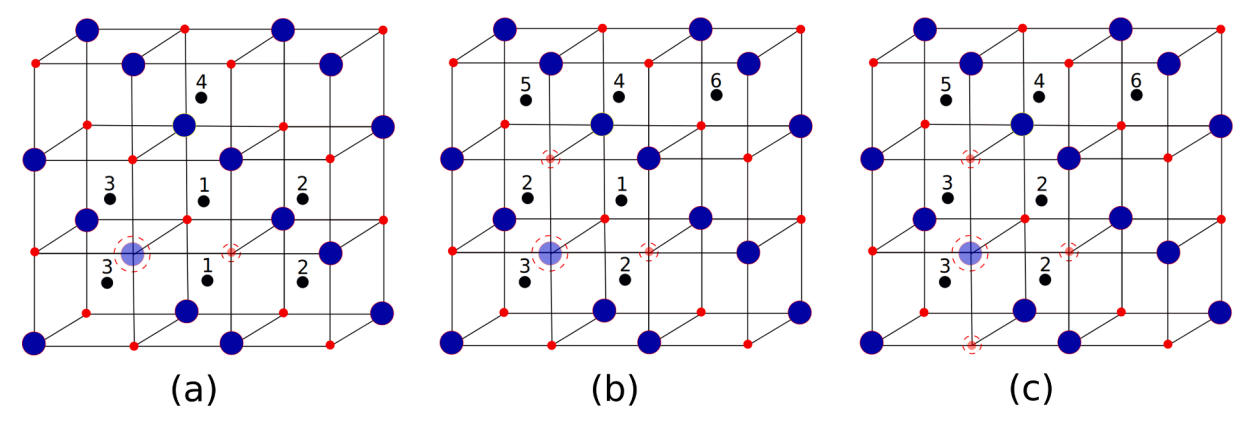


Fig. 9. The potential off-lattice interstitial positions for (a)  $Me_v - C_v - I$  (b)  $Me_v - 2C_v - I$  and (c)  $Me_v - 3C_v - I$  defect clusters.

**Table 4**The change in energy for the off-lattice configurations relative to their most energetically favorable on-lattice configurations.

Mechanism	Interstitial	TiC	ZrC	HfC	VC	NbC	TaC
$Me_{\nu} - C_{\nu} - I$ Fig. 9(a)	Octahedral	1.05	2.32	1.36	1.74	2.78	_
	1	-1.63	-1.49	-0.85	-0.30	0.72	2.11
	2	0.87	1.73	2.39	1.25	2.78	3.99
	3	-2.07	-1.55	-0.95	-0.63	0.61	2.34
	4	1.63	1.24	2.14	2.41	3.56	5.17
$Me_v - 2C_v - I$ Fig. 9(b)	Octahedral	-0.89	-0.88	-0.19	0.83	1.57	3.90
	1	-0.30	-0.06	0.44	0.27	0.89	1.88
	2	-1.02	-0.94	-0.89	0.06	0.95	2.17
	3	-1.47	-0.69	-0.75	-0.18	0.97	2.74
	4	1.42	0.69	2.45	1.90	3.10	4.71
	5	1.21	0.74	1.80	1.52	3.14	4.67
	6	2.06	2.80	3.53	3.01	4.31	5.60
$Me_v - 3C_v - I$ Fig. 9(c)	Octahedral	1.14	0.98	1.57	0.38	2.82	_
	2	-0.01	0.25	0.79	0.50	0.93	1.86
	3	-0.96	-0.76	-0.08	0.27	1.04	2.25
	4	1.77	2.56	2.77	2.03	3.19	4.36
	5	1.55	2.13	2.78	1.64	3.25	4.34
	6	2.33	3.11	3.83	3.12	4.39	6.12

atoms, leaving some of the carbon atoms with non-ideal broken covalent bonds. Thus, if a carbon atom is moved from its normal lattice position, which is no longer ideally bonded, into the tetrahedral position, it is able to create covalent bonds with carbon atoms around it and this formation more preferential if the carbon atoms around it have their covalent metal–carbon bonds broken by the metal vacancy. This bond formation concept is backed up by the fact that the resulting carbon–carbon bond length is 0.149 nm (for a carbon interstitial in ideal TiC) compared to the ideal single carbon bond length of 0.154 nm in diamond. Thus, we anticipate that the most favorable off-lattice position will sit in interstitial sites that have a maximum number of carbon–carbon bonds (making it "ideally tetrahedrally coordinated") as well as a maximum number of broken Me-C bonds of the on-lattice carbon atoms surrounding the interstitial.

We can test this idea by comparing the formation energies for different configurations. For example, site 3 in Fig. 9(a), which has the largest decrease in formation energy, indeed maximizes the broken Ti-C covalent bonds around the interstice, which is two, and maximizes the number of carbon bonds at four. Site 1 is adjacent to two carbon atoms whose Ti-C covalent bonds are broken by the missing carbon atom but is only surrounded by three other carbon atoms and is thus higher formation energy. Similar trends are observed for the other configurations in Fig. 9. It is not possible to claim one of the two factors is more important, because some of favorability between the two lowest energy sites varies with chemistry, but this does help explain why these sites become energetically favorable. We can see that the favorability of this mechanism depends both on the number of valence electrons as well as

the shell involved in the bonding, as this formation energy becomes less favorable both with an increase in the number of valence electrons as well as the number of the shell (i.e. 4d vs. 5d vs. ...) involved in bonding resulting in these sites being most unfavorable in TaC.

Table 5 lists the formation energies of the most favorable off-lattice positions for these new defect complexes in the Ti-C system. Similar decreases are found in the Zr-C and Hf-C systems. These reductions in the metal formation energy suggests that this mechanism may be the primary mechanism of diffusion as long as the migration energies are sufficiently small. Thus, it is important to consider nature of carbon atom diffusion associated with these vacancy-interstitial clusters. Since

**Table 5**Activation Energies for the off-lattice migration mechanisms considered in this paper.

TiC		$E_f$ (eV)	$E_m$ (eV)	Q (eV)
Experiment $Me_{ u} - C_{ u} - I$	Path 1	5.60	5.40	7.64 <sup>a</sup> 11.00
$Me_{\nu}-2C_{\nu}-I$	Path 2	5.60	4.14	9.74
	Path 1	4.75	3.95	8.70
$Me_{\nu}-3C_{\nu}-I$ (line)	Path 2	4.75	3.55	8.30
	Path 1	4.12	3.76	7.88
$Me_{\nu} - 3C_{\nu} - I$ (triangle)	Path 2	4.12	3.94	8.06
	Path 1	4.12	3.66	7.78
	Path 2	4.12	4.34	8.46

<sup>&</sup>lt;sup>a</sup>Ti in TiC<sub>0.97</sub> [22].

the off-lattice positions are not favorable for either TaC and NbC, we did not examine the migration of these defects in the group VB carbides.

## 3.2.2. Migration mechanisms

In order to understand and quantify the mechanisms of diffusion associated with these new vacancy configurations, we considered the lowest energy configurations associated with the  $Me_{\nu}-C_{\nu}-I$ ,  $Me_v - 2C_v - I$ , and  $Me_v - 3C_v - I$  defect clusters as the initial configurations. While there exist several sequences of atomic jumps that might give rise to the migration of these clusters, we choose two representative sequences of jumps for each mechanism to capture the representative migration energies. We limit our search to just two sequences for each configuration due to the expensive nature for the simulations; each path consists of at least five different NEB simulations comprising of nine images each with over 120 atoms per image. We consistently choose these two paths so that each path has a specific metal atom migration. When the metal migrates, path 1 has no carbon atoms in the off-lattice positions while path 2 has one carbon in the off-lattice position. This is done because the coordination of the off-lattice carbon atom, with the metal atom, likely will influence the energetics of migration and we wanted to ensure we sampled both possibilities.

Metal vacancy with carbon vacancy-interstitial pair  $(Me_v - C_v - I)$ 

For the  $Me_v-C_v-I$  lowest energy state, the two different jump sequences chosen are shown in Fig. 10(a). Path 1 consist of the atomic jumps i-ii-iii-iv-v while path 2 consists of the jumps iii-ii-ii-v-v. Fig. 10(b) reveals the minimum energy paths for each of the sequences of jumps for path 1 and 2. The migration energy barrier for path 1 is 5.40 eV and for path 2 is 4.14 eV. This results in a total activation energy for diffusion along path 1 and 2 of 11.00 eV and 9.74 eV, respectively. This activation energy is much lower than the activation energy of a single isolated metal vacancy studied previously even though both have the same number of atoms.

Di-vacancy with carbon vacancy-Interstitial pair (Me $_v$   $-2C_v$  -I).

The two atomic migration paths for the  $Me_v - 2C_v - I$  defect cluster are shown in Fig. 11(a), which correspond to the jump sequences of i-ii-iii-iv-v and i-iii-ii-iv-v, respectively. Fig. 11(b) shows the minimum energy paths for path 1 and path 2 and with migration energy barriers being 3.95 eV and 3.55 eV, respectively. Combing these migration energy barriers with the metal vacancy formation energy results in activation energies for path 1 and path 2 of 8.70 eV and 8.30 eV. Thus, the  $Me_v - 2C_v - I$  mechanism provides an activation energy lower than the activation energy of the di-vacancy pair (10.17 eV and 11.44 eV) and is

much closer to the experimentally reported activation energy for metal atom migration in TiC (7.64 eV) [5].

Tri-vacancy with carbon vacancy-Interstitial pair  $(Me_v - 3C_v - I)$  Fig. 12(a) shows the two chosen migration paths for the  $Me_v - 3C_v - I$  defect cluster for path 1 and path 2, which consist of the atomic jump sequences i-ii-iii-iv-v and i-iii-iiv-v, respectively. The sequence of path 1 is chosen such that, in the intermediate steps of migration, two-carbon vacancies and one metal vacancy form a line configuration as shown by the position 1 and 3 in Fig. 3(a). The minimum energy path for these jump sequences are shown in Fig. 12(b), which gives a migration energy barrier of 3.76 eV and 3.94 eV for paths 1 and 2 respectively. Combining this migration energy barriers with the metal formation energy determined for  $Me_v - 3C_v - I$  (line) cluster mechanism, the activation energies for these processes are 7.88 eV and 8.06 eV for paths 1 and 2. An additional set of migration paths can be found in the Supplemental Information.

Table 5 tabulates all of the computed activation energies for the different off-lattice migration mechanisms. As noted, the activation energies found in  $Me_v - 3C_v - I$  mechanism results in activation energies consistent with experiments in TiC (7.64 eV) [22]. Fig. 13 shows a comparison of the activation energies for Ti diffusion in TiC for our onlattice and off-lattice model as a function of the net carbon vacancy concentration with the activation energies computed from the experiments of Sarian et al. [22] and statistical study of Tang et al. [36], respectively. Generally speaking, we see that the activation energy of the off-lattice model is lower than the on-lattice models and approaches the value of the experiments for two net carbon vacancies which corresponds to the  $Me_v - 3C_v - I$  defect complex. In that context, this work generally shows that the off-lattice configurations have lower activation energies for the same net number of carbon vacancies as well as correspondingly lower formation energies than the on-lattice model. Thus, we can conclude that the off-lattice model is much more likely mechanism of metal vacancy migration in TiC in specific and the group IVB carbides in general.

The work of Tang et al. [36] demonstrated that, when considering the statistics associated with the vacancy formation and migration mechanisms, the most probably states were the  $Me_v - 4C_v$  and  $Me_v - 5C_v$  vacancy clusters (on lattice) in TiC, demonstrating that the lowest format energy associated with the  $Me_v - 6C_v$  vacancy cluster mechanism is not the most influential mechanism. Thus, it is not critical to search for the absolute lowest activation energy combination since the statistic play an important role. Our results have similar formation and migration

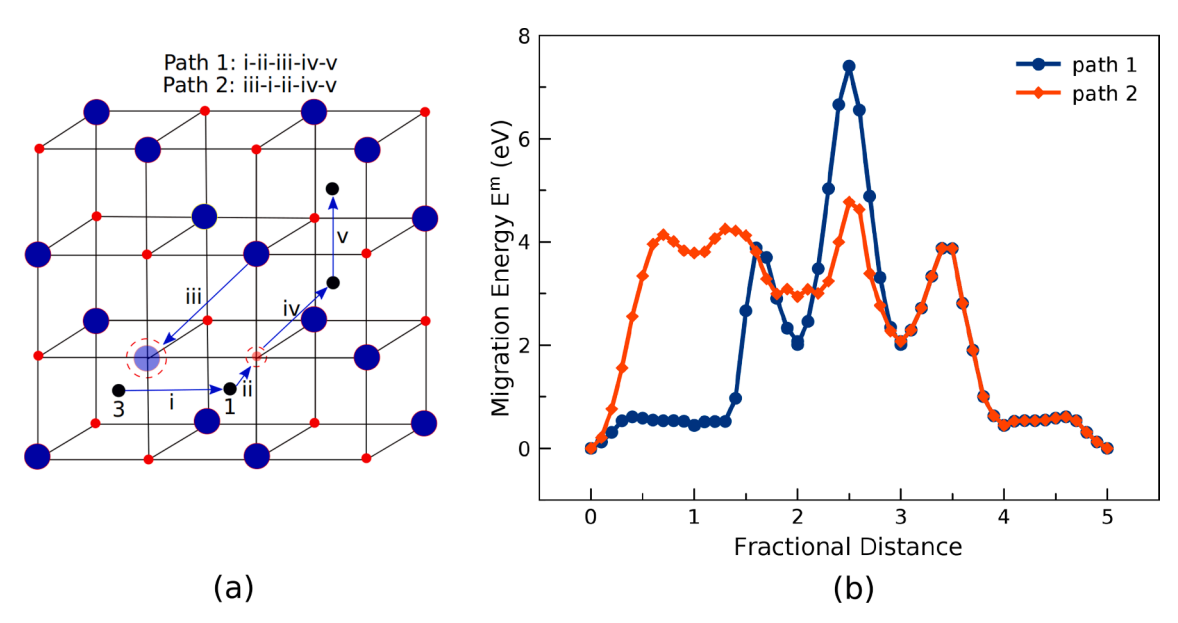


Fig. 10. (a) The atomic jump sequence and (b) the minimum energy path for path 1 and path 2 in the  $Me_v - C_v - I$  diffusion mechanism in TiC.

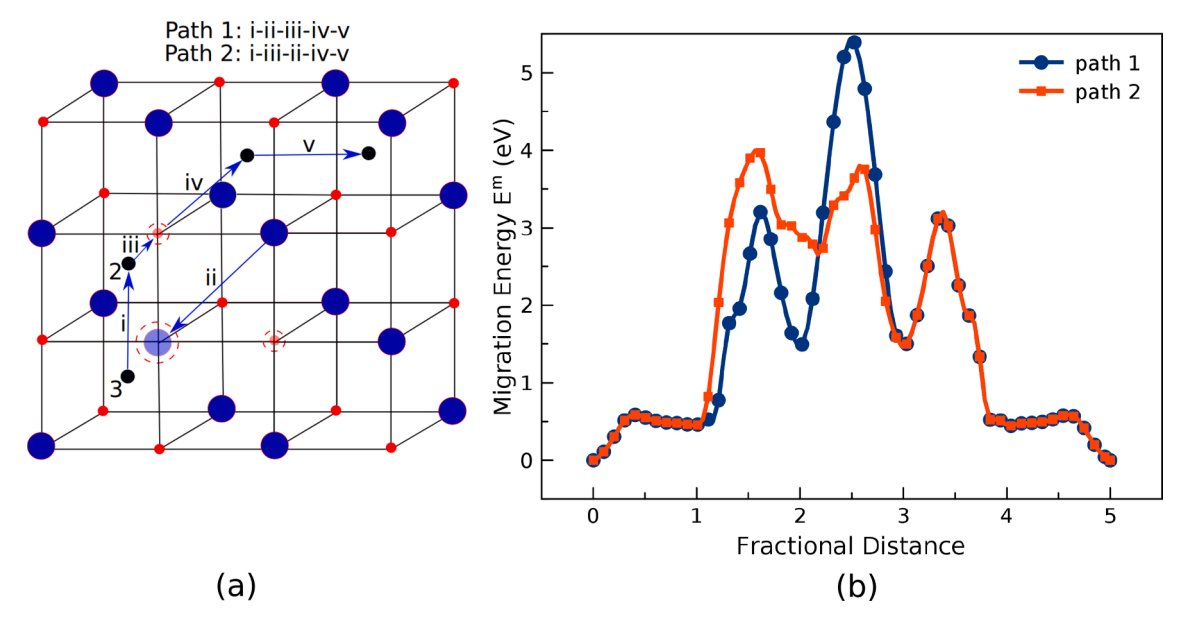
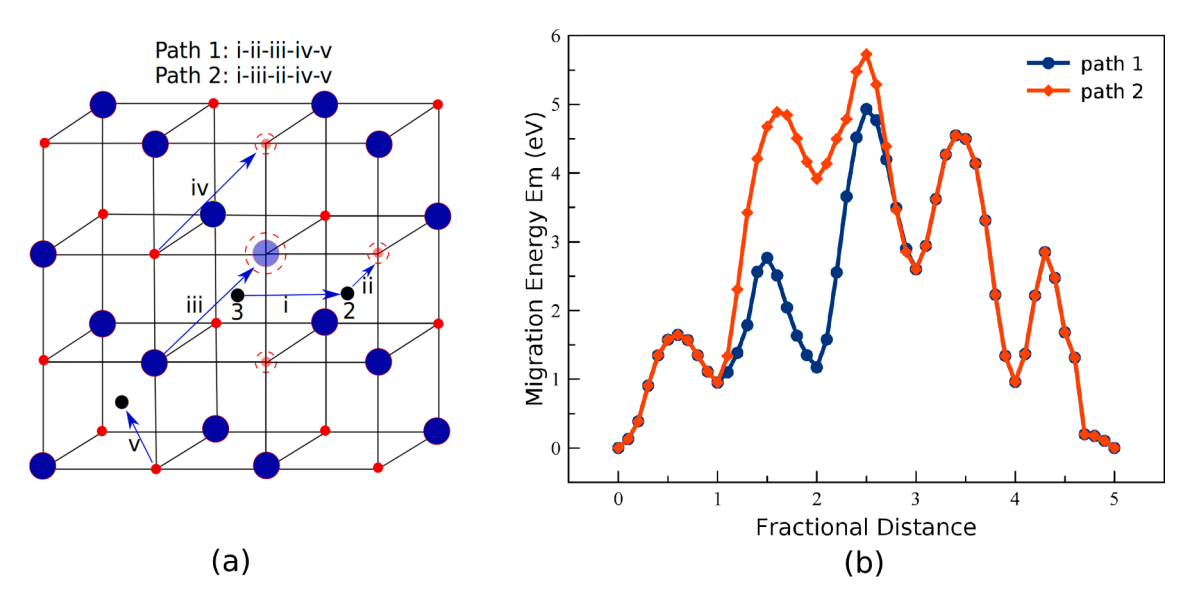


Fig. 11. (a) The atomic jump sequence and (b) the minimum energy path for path 1 and path 2 in the  $Me_v - 2C_v - I$  mechanism in TiC.



**Fig. 12.** (a) The atomic jump sequence for vacancies with line configuration in the intermediate step of migration and (b) the migration energy barrier for path 1 and path 2 in the  $Me_v - 3C_v - I$  (line) cluster mechanism in TiC.

energy barriers as those reported by Sun et al. [26], who studied metal atom interstitial migration, and we expect that both mechanisms contribute to mass diffusion in the group IVB carbides.

Finally, it is worth putting forth an interpretation of these results. Our identified mechanism is referenced to the off-lattice interstitial positions which results in relatively deformed local atomic positions. With thermal motion, it is very likely that these defect complexes will appear less ordered and more disordered, especially at higher temperatures. Therefore, our results suggest that the metal atom vacancy will appear as a very local atomic disorder in the lattice.

## 4. Summary and conclusions

In this work, we computed the formation energies and migration energy barriers for vacancy clusters in the group IVB and VB transition metal carbides. The formation energies of vacancy defect clusters demonstrate a clear difference between the two groups. There is a strong binding energy between metal and carbon vacancies that enhances the

formation of metal—carbon vacancy clusters that is much less prominent in the group VB carbides. This results in the formation energy of a metal atom in the group IVB carbides achieving a minimum when the metal atom is surrounded by six carbon atoms. However, the minimum in the metal vacancy formation energy for the group VB carbides occurs when the metal vacancy is only surrounded by two carbon vacancies.

This work has also demonstrated that carbon atom diffusion in the group IVB and VB carbides can also occur through the tetrahedral interstices. This is the lowest energy carbon migration path for most chemistries and vacancy concentrations, which has not been previously reported. Furthermore, the  $Me_{\nu}$  –6 $C_{\nu}$  does indeed have the lowest activation energy for all of the considered on-vacancy paths in TiC, but not in TaC. As pointed out by Tang et al. [36] despite this lower activation energy, statistically it does not contribute to diffusion in nearly stoichiometric carbides.

The minimum energy paths studied in our on-lattice model found in the group IVB carbides revealed that some of the tetrahedral and octahedral carbon interstitial positions have lower energies than the initial

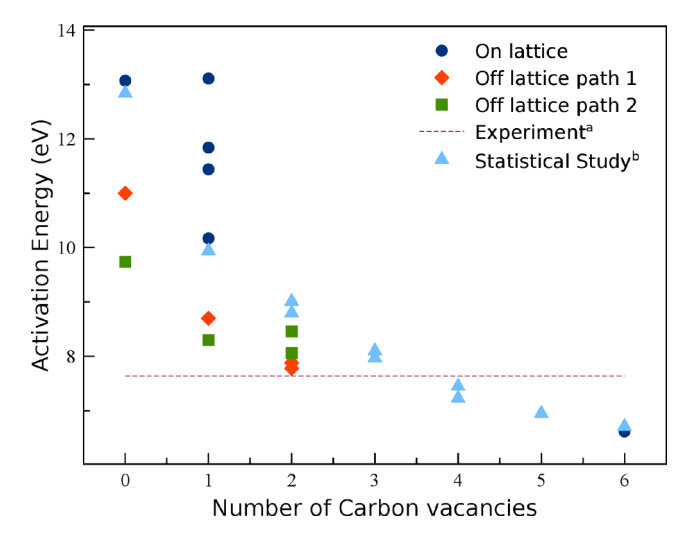


**Fig. 13.** Comparison of activation energies of our on-lattice and off-lattice migration with previous experimental and statistical studies in TiC.  $^{a}$ Experimental diffusion measurements for Ti in TiC<sub>0.97</sub> [22] and  $^{b}$ the activation energies of the simple model proposed by Tang et al. [36].

on-lattice positions; the same positions are unfavorable in group VB carbides. A thorough study of the defect energetics of these vacancy-interstitial clusters demonstrate that they have markedly lower formation energies than the on-lattice configurations, which extends at least up to  $Me_{\nu}-3C_{\nu}-I$  compositions. Given these very low formation energies, these are the most probable defect states for metal vacancies.

The NEB simulations of atomic migration show a plethora of different migration paths that give rise to a range of potential activation energies which are not substantially different from the on-lattice barriers. Due to the lower formation energies, the activation energies associated with the off-lattice configurations are indeed lower than the on-lattice configurations suggesting that these off-lattice configurations are the likely configuration of metal vacancy clusters and thus the most important configuration to consider for mass diffusion in the group IVB carbides. We contrast this finding in the group VB carbides (TaC and NbC) which, due to the higher formation energies of the off-lattice configurations, most likely diffuse by a bound di-vacancy pair [36]. This, in conjunction with the studies of Sun et al. [26], suggest that mass diffusion in the group IVB carbides will most likely appear as local disordered defect clusters that move through the lattice. Finally, we note that our results are largely applicable near the MeC<sub>1,0</sub> chemistry as all the vacancy formation energies, migration barriers, and chemical potentials were evaluated near this chemistry. Further work is needed to understand how these mechanisms would change with substantial changes in stoichiometry as is possible in many of the transition metal carbides.

## **Declaration of Competing Interest**

The authors declare that they have no known competing financial interests or personal relationships that could have appeared to influence the work reported in this paper.

## Acknowledgments

This work utilized the RMACC Summit supercomputer, which is supported by the National Science Foundation (awards ACI-1532235  $\,$ 

and ACI-1532236), the University of Colorado Boulder and Colorado State University. The RMACC Summit supercomputer is a joint effort of the University of Colorado Boulder and Colorado State University. G.B. T. recognizes NSF-DMR-2026760 and C.R.W. recognizes NSF-DMR-2026766 for additional support.

#### Appendix A. Supplementary data

Supplementary data associated with this article can be found, in the online version, at https://doi.org/10.1016/j.commatsci.2021.110713.

#### References

- [1] L. Toth, Transition Metal Carbides and Nitrides, Elsevier, 2014.
- [2] W.S. Williams, Science 152 (1966) 34-42.
- [3] G.B. Thompson, C.R. Weinberger, Ultra-High Temperature Ceramics: Materials for Extreme Environment Applications (2014) 291–315.
- [4] Y.V. Miloserdin, K. Naboichenko, L. Laveikin, A. Bortsov, Strength of Materials 4 (1972) 302–305.
- [5] R. Steinitz, Nuclear Applications of Non-Fissionable Ceramics (1966) 75–100.
- [6] F. Keihn, R. Kebler, Journal of the Less Common Metals 6 (1964) 484-485.
- [7] J. Chermant, G. Leclerc, B.L. Mordike, Zeitschrift fuer Metallkunde 71 (1980) 465–469.
- [8] I. Spivak, R. Andrievskii, V. Rystsov, V. Klimenko, Soviet Powder Metallurgy and Metal Ceramics 13 (1974) 574–578.
- [9] W. Brizes, 1968.
- [10] C.J. Smith, M.A. Ross, N. De Leon, C.R. Weinberger, G.B. Thompson, Journal of the European Ceramic Society 38 (2018) 5319–5332.
- [11] D. McLean, Reports on Progress in Physics 29 (1966) 1.
- [12] S. Sarian, Journal of Applied Physics 39 (1968) 3305-3310.
- [13] S. Sarian, Journal of Applied Physics 39 (1968) 5036-5041.
- [14] D. Kohlstedt, W.S. Williams, J. Woodhouse, Journal of Applied Physics 41 (1970) 4476–4484.
- [15] V. Eremeev, A. Panov, Soviet Powder Metallurgy and Metal Ceramics 6 (1967) 306–309.
- [16] S. Sarian, Journal of Physics and Chemistry of Solids 33 (1972) 1637–1643.
- [17] W.F. Brizes, L. Cadoff, J. Tobin, Journal of Nuclear Materials 20 (1966) 57–67.
- [18] R. Resnick, R. Steinitz, L. Seigle, Transactions of the Metallurgical Society of AIME 233 (1965) year.
- [19] X.-X. Yu, G.B. Thompson, C.R. Weinberger, Journal of the European Ceramic Society 35 (2015) 95–103.
- [20] B. Yu, R.F. Davis, Journal of Physics and Chemistry of Solids 42 (1981) 83–87.
- [21] R.F. Davis, Diffusion and Creep in Niobium Carbide as a Function of Temperature and Carbon Content., North carolina state university, raleigh (usa). Department of Engineering Research Technical Report, 1981.
- 22] S. Sarian, Journal of Applied Physics 40 (1969) 3515–3520.
- [23] P. Andrievskij, Y.F. Khromov, I. Alekseeva, Fizika Metallov i Metallovedenie 32 (1971) 664–667.
- [24] V.I. Razumovskiy, P.A. Korzhavyi, A.V. Ruban, Solid State Phenomena (2011) 990–995.
- [25] V.I. Razumovskiy, A.V. Ruban, J. Odqvist, P.A. Korzhavyi, Physical Review B 87 (2013), 054203.
- [26] W. Sun, H. Ehteshami, P.R. Kent, P.A. Korzhavyi, Acta Materialia 165 (2019) 381–387.
- [27] W. Sun, H. Ehteshami, P.A. Korzhavyi, Physical Review B 91 (2015), 134111.
- [28] G. Kresse, J. Hafner, Physical Review B 47 (1993) 558.
- [29] G. Kresse, J. Furthmüller, Physical Review B 54 (1996) 11169.
- [30] G. Kresse, J. Hafner, Physical Review B 49 (1994) 14251.
- [31] P.E. Blöchl, Physical Review B 50 (1994) 17953.
- [32] G. Kresse, D. Joubert, Physical Review B 59 (1999) 1758.
- [33] J.P. Perdew, J. Chevary, S. Vosko, K.A. Jackson, M.R. Pederson, D. Singh, C. Fiolhais, Physical Review B 48 (1993) 4978.
- [34] J.P. Perdew, K. Burke, M. Ernzerhof, Physical Review Letters 77 (1996) 3865.
- [35] H.J. Monkhorst, J.D. Pack, Physical Review B 13 (1976) 5188.
- [36] X. Tang, R. Salehin, G.B. Thompson, C.R. Weinberger, Physical Review Materials 4 (2020), 093602.
- [37] H. Yu, M. Guziewski, G.B. Thompson, C.R. Weinberger, Modelling and Simulation in Materials Science and Engineering 24 (2016), 055004.
- [38] V. Razumovskiy, M. Popov, H. Ding, J. Odqvist, Computational Materials Science 104 (2015) 147–154.
   [39] G. Henkelman, B.P. Uberuaga, H. Jóson, The Journal of Chemical Physics 113
- (2000) 9901–9904.

  [40] W. Cai, W.D. Nix, Imperfections in Crystalline Solids, Cambridge University Press,
- [41] N.S. Weingarten, E.F. Byrd, Computational Materials Science 96 (2015) 312–318.